Atmospheric
Measurement
Techniques

An inverse-modelling approach for frequency response correction of capacitive humidity sensors in ABL research with small remotely piloted aircraft (RPA)

N. Wildmann, F. Kaufmann, and J. Bange

Center for Applied Geoscience, Eberhard Karls Universität Tübingen, Tübingen, Germany

Correspondence to: N. Wildmann (norman.wildmann@uni-tuebingen.de)

Abstract. The measurement of water vapour concentration in the atmosphere is an ongoing challenge in environmental research. Satisfactory solutions exist for ground-based meteorological stations and measurements of mean values. However, carrying out advanced research of thermodynamic processes aloft as well, above the surface layer and especially in the atmospheric boundary layer (ABL), requires the resolution of small-scale turbulence. Sophisticated optical instruments are used in airborne meteorology with manned aircraft to achieve the necessary fast-response measurements of the order of 10 Hz (e.g. LiCor 7500). Since these instruments are too large and heavy for the application on small remotely piloted aircraft (RPA), a method is presented in this study that enhances small capacitive humidity sensors to be able to resolve turbulent eddies of the order of 10 m. The sensor examined here is a polymer-based sensor of the type P14-Rapid, by the Swiss company Innovative Sensor Technologies (IST) AG, with a surface area of less than 10 mm^2 and a negligible weight. A physical and dynamical model of this sensor is described and then inverted in order to restore original water vapour fluctuations from sensor measurements. Examples of flight measurements show how the method can be used to correct vertical profiles and resolve turbulence spectra up to about 3 Hz. At an airspeed of 25 m s^{-1} this corresponds to a spatial resolution of less than 10 m.

1 Introduction

1.1 Water vapour in atmospheric research

The atmospheric boundary layer (ABL) is in direct contact with the Earth surface and subject to water exchange with the soil, rivers, lakes and oceans. Although it is decoupled by a temperature inversion from the free atmosphere, entrainment processes lead to an exchange of water vapour through the inversion (Stull, 1988). This exchange of water, enforced by turbulent transport in the ABL, leads to a high temporal, horizontal and vertical variability of water vapour. Water vapour concentration is not only important for cloud formation, rainfall and fog; it also plays an important role in the energy balance of the Earth surface and for thermodynamic processes in the atmosphere. Recent large-eddy simulations (LES) showed how the structure parameter of humidity is much less understood than the structure parameter of temperature. The structure parameter, or structure function parameter (Stull, 1988), is a characteristic parameter of a turbulent signal in the locally isotropic subrange and can also be used to estimate fluxes of the corresponding quantities (Wyngaard and Clifford, 1978). The ABL structure is typically described by means of similarity theories and parametrizations (Garratt, 1992) in order to compare results in different regimes. While for example the Monin–Obukhov similarity theory is found to be valid in all regimes for temperature, the same theory does not apply to humidity, especially if entrainment into the mixed layer is present (Maronga, 2013). A more detailed description of entrainment processes is needed, which will need precise measurements of water vapour fluxes to validate the models. Recently, first

measurements of entrainment processes with small remotely piloted aircraft (RPA) were reported (Martin et al., 2013), but only temperature and wind could be analysed, due to a lack of fast-response humidity measurements. Essential for the measurement of turbulent fluctuations is a high sampling rate and a short time response throughout the measurement chain, high measurement resolution and high accuracy. One goal of this study is to provide a method to enhance present sensors on small RPA in order to make the required measurements in the ABL.

1.2 Water vapour measurement in airborne systems

In situ measurement of atmospheric processes above the surface layer requires airborne sensor carriers in the form of fixed-wing aircraft, helicopters, balloons or similar. There are research aircraft for upper-troposphere and lower-stratosphere measurements, but also for measurements in the ABL, which are the focus of this study. Examples of research aircraft for boundary-layer research are the Dornier 128 (Bange et al., 2002; Corsmeier et al., 2001) and the MetAir Dimona (Neininger et al., 2001). A slightly different type of airborne system that was used for ABL research is the helicopter probe Helipod (Bange and Roth, 1999). All of them carry at least one instrument to investigate water vapour and its fluxes in the ABL. An overview of the state of the art of instrumentation for airborne measurements is given in Bange et al. (2013), and a short summary is presented in Sect. 2.1 of this article. It should be noted that manned research aircraft are subject to high operating costs and thus are only used in short, dedicated field experiments. Within the last decade, technical progress has made it possible to use small RPA, equipped with autopilots and way-point navigation, for research purposes in many fields (Martin et al., 2011, 2013; Martin and Bange, 2013; van den Kroonenberg et al., 2011, 2008; Spieß et al., 2007; Jonassen, 2008; Chao et al., 2008; Jensen and Chen, 2013). Their flexibility and low operating cost enables researchers to come up with new, innovative ideas to probe the atmosphere in a way that was not possible before. Along with these possibilities come the challenges of making instrumentation even smaller and more lightweight in order for it to be carried on these aircraft while still competing with the quality of ground-based sensors. The smallest of these unmanned aerial vehicles (UAVs), as they are also called, weigh up to 5 kg and carry capacitive humidity sensors of different kinds (Reuder et al., 2009; Martin et al., 2011). Larger RPA, up to 50 kg, can carry more sophisticated sensors that are too large for the smaller RPA, such as krypton hygrometers (Thomas et al., 2012). Small RPA have several advantages: it is comparatively easy to obtain flight permission for them in central Europe. They do not require special ground facilities, such as a catapult or a runway, and they are low-cost. Furthermore, small RPA do not disturb the turbulent flow they have to measure, which increases accuracy, while, at the same time, the

sensors allow a fast-response measurement of the variable of interest. This shows that an improved response time for capacitive humidity sensors can be of great benefit for atmospheric research and especially for turbulence measurements. The University of Tübingen operates the RPA MASC (Multi-purpose Airborne Sensor Carrier), which is equipped with fast temperature sensors (Wildmann et al., 2013), a flow probe (Wildmann et al., 2014) and a capacitive humidity sensor. All flight measurements that are presented in this article were carried out with the MASC RPA.

1.3 Control theory and signal restoration

In this study, methods of control theory will be applied to achieve better results in the measurement of humidity with capacitive sensors. In control theory, mathematical models are derived from physical systems and put into standard forms to describe the dynamics of the system and to eventually design controllers to influence the system's behaviour. Instead of designing controllers for the system, the mathematical description of the dynamic behaviour of the system can also be used to restore the original signal from a measurement if the dynamics of the sensor are well described. Similar work has been done in the field of airspeed measurement with flow probes (Rediniotis and Pathak, 1999) to correct for time delays in the pneumatic setup of these sensors. Another example are thermocouples in combustion engines where fast response of the sensors in harsh conditions is desired (Tagawa et al., 2005). It is shown in this report how similar techniques can be applied for capacitive humidity sensors in ABL research. Compared to simple time delay corrections that were reported to be applied to capacitive humidity sensors in radiosondes (Leiterer et al., 2005; Miloshevich et al., 2004), the approach using control theory methods makes it possible to better understand the dynamics that are found for this type of sensor.

2 Water vapour measurement

2.1 State of the art

A variety of sensors is used to measure water vapour concentration in the atmosphere. Polymer-based absorption hygrometers are used for observations of relative humidity in most modern weather stations, where a fast response time is not an issue (Kuisma et al., 1985). Some of the most common and most modern radiosondes are the Vaisala RS92, GRAW DFM-09 and Modem M10. All of them carry capacitive, polymer-based humidity sensors and claim fast response times. However, radiosondes are designed to provide accurate vertical profiles but only limited information about turbulence. Their sampling rate is usually of the order of 1 Hz, the resolvable frequencies much lower. The most widely used instrument for ground-based flux measurements is the LI-7500A gas analyser by the company Li-Cor® (Eckles, 2001).
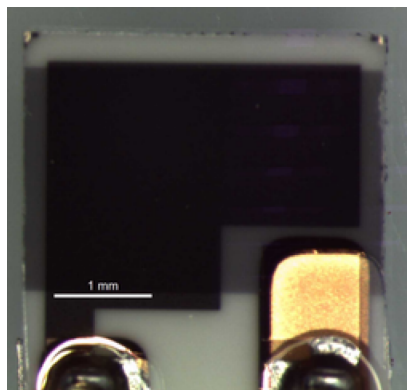
Figure 1. Sensitive element of a capacitive humidity sensor. The black polygon is the polymer between two gold electrodes.

Table 1. Overview of P14 Rapid characteristics.

Size	approx. 3×2 mm
Active element area	6×10^{-6} m^2
Thickness	1 μm
Material	unknown polymer
Specified response time	< 1.5 s

In airborne measurements, a wide variety of customized instruments is being used, including, e.g., Lyman-α absorption hygrometers (e.g. Buck, 1976; Bange et al., 2002), tunable diode laser absorption spectroscopy hygrometers (TDLAS, e.g. May, 1998; Zondlo et al., 2010; Paige, 2005), infrared absorption hygrometers (e.g. LI-7500A), chilled-mirror dew point instruments (DPM, Neininger et al., 2001), krypton hygrometers (Campbell et al., 1985; Thomas et al., 2012) or polymer-based thin-film capacitive absorption hygrometers (see Spieß et al., 2007; Reuder et al., 2009). Only the optical instruments are usually used for turbulence analysis.

Additional sensor types that have not previously been mentioned and are found in ground-based meteorology are psychrometers and resistive or inductive hygrometers.

2.2 Capacitive humidity sensors

None of the instruments that are used on manned aircraft can easily be carried by small RPA, where compact size and light weight are essential. A trade-off has to be made regarding accuracy, response time and long-term stability of the sensors. Considering all the sensor types mentioned in Sect. 2.1, only the capacitive humidity sensor can be easily integrated into a small RPA with current state of the art technology. The size of these elements is typically less than 1 cm^2, and, in non-severe conditions, accuracy and stability of the elements is adequate.

Table 2. List of tested polymer-based humidity sensors

Model	Company
P14 Rapid	IST AG
G-US.171R2	U.P.S.I.
HIH4030	Honeywell
HYT-241	Hygrosens
SHT75	Sensirion
HMP50	Vaisala
DigiPicco	IST AG
HTM-B71	Tronsens

Capacitive humidity sensors are in most cases based on thin-film polymers (Tetelin and Pellet, 2006; Sen and Darabi, 2008; Shibata et al., 1996). The materials adsorb water at the sensor surface from where it diffuses into the material and changes the relative permittivity and therefore the capacitance of the sensor (see Sect. 2.3). With decreasing thickness of the polymer, the time constant also decreases. One of the fastest of this kind on the market is the P14 Rapid by Innovative Sensor Technology (IST) AG (Fig. 1, Table 1), which has a time response of < 1.5 s falling edge, according to the specification (IST AG, 2009). Other sensors that are commercially available and were tested, both in a climate chamber and in flight, are listed in Table 2. The sensors HYT-241, HTM-B71, SHT75 and DigiPicco have a digital output that only allows low sampling rates. HIH4030 and HMP50 are analogue sensors. All of these sensors showed a slower time response than the P14 Rapid. The G-US.171R20 did show a very fast response to humidity changes but was extremely sensitive to temperature changes as well. The calibration of this sensor was not found to be stable in the long term.

Polymer sensors can be subject to hysteresis, as adsorption and desorption do not necessarily take place at the same rate. They also might show a certain temperature sensitivity. A quantification of these effects needs to be done for each sensor type, since the effects can differ a lot depending on the dielectric material and the design of the element. The P14 Rapid sensor was found to be the fastest sensor available and showed little hysteresis and temperature sensitivity. All experiments were carried out using this particular sensor. The polymer type is a trade secret, thus parts of the model derived in Sect. 2.3 rely on experimental parameter estimation. The polymer thickness of 1 μm was obtained from IST (F. Krogmann, personal communication, 2012). In the setup that was used for this study, the sensor is connected to the PCAP01 capacitance converter chip on a custom-made printed circuit board (PCB, see Fig. 2). The converter measures the charge and discharge time of the capacitor in comparison to a known reference capacitance and provides the ratio of the two on a digital output. The digital signal is then processed by the AMOC (Airborne Meteorological Onboard Computer), which was developed at the University of
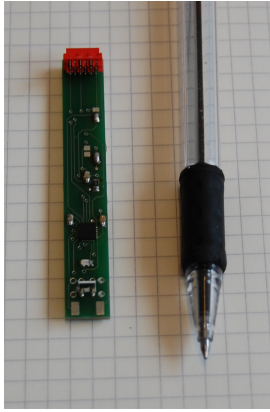
Figure 2. Humidity sensor on printed circuit board with the capacitance measurement chip PCAP01.

Applied Sciences Ostwestfalen-Lippe and the University of Tübingen. The computer stores the data at 100 Hz onto an SD card. At the same time, the sensor signal can be monitored in real time on a remote computer.

In order to better understand the measurements that are done with the P14 Rapid, Sect. 2.3 introduces a model which relates the measured capacitance to the water concentration in the polymer. In a steady state, the water concentration in the polymer equals the water concentration at the sensor surface. Section 2.4 introduces a calibration to get the relative humidity from the surface water concentration. Finally, Sect. 3 describes how the diffusion process of water from the sensor surface into the polymer can be modelled and how, by inversion of this model, the surface concentration of the sensor – and thus the ambient relative humidity – can be estimated throughout a measurement flight.

2.3 Physical model

In Sect. 3, a dynamical model will be presented, which describes the change of water concentration in the polymer with time. In order to work with this model, it is necessary to translate the measurement variable capacitance C to the corresponding average water concentration in the polymer c. In this section, a physical model is presented, which describes this relation. In a parallel-plate capacitor, the charge per voltage is defined as the capacitance. It can also be expressed as a function of the area A of the parallel plate, the distance d between the plates, the relative permittivity ε_r of the material between the plates and the vacuum permittivity ε_0:

$$C = \frac{Q}{U} = \varepsilon_0 \varepsilon_r \frac{A}{d} = (\varepsilon_r - 1)\varepsilon_0 \frac{A}{d} + \varepsilon_0 \frac{A}{d}. \quad (1)$$

For the following investigation, it helps to decompose the capacity of the humidity sensor into partial capacities (Eq. 2), in particular the capacitance of the vacuum between the plates C_0, the capacitance of the polymer alone C_{Poly} and the capacitance of absorbed water in the polymer $C_{\text{H}_2\text{O}}$. C_{Poly}

and C_0 are constant and provide an offset capacitance for zero water concentration, while $C_{\text{H}_2\text{O}}$ accounts for the sensitivity of the capacitance to changes in water concentration in the polymer.

$$C = \varepsilon_0(\varepsilon_r^{\text{H}_2\text{O}} + \varepsilon_r^{\text{Poly}})\frac{A}{d}$$
$$= \underbrace{\varepsilon_0 \varepsilon_r^{\text{Poly}} \frac{A}{d}}_{:= C_{\text{Poly}}} + \underbrace{(\varepsilon_r^{\text{H}_2\text{O}} - 1)\varepsilon_0 \frac{A}{d}}_{:= C_{\text{H}_2\text{O}}} + \underbrace{\varepsilon_0 \frac{A}{d}}_{:= C_0}. \quad (2)$$

The Debye equation for molar polarisation P_m connects the microscopic characteristics, which are the electrical dipole moment μ and the polarizability α, to the relative permittivity ε_r of a material (Debye, 1929).

$$P_m = \frac{\varepsilon_r^{\text{H}_2\text{O}} - 1}{\varepsilon_r^{\text{H}_2\text{O}} + 2} = \frac{Z}{3\varepsilon_0} \cdot \left(\alpha + \frac{\mu^2}{k_B T}\right), \quad (3)$$

with particle density $Z = \frac{\varrho}{M} N_A$ and ϱ being the density, M the molecular mass, N_A the Avogadro constant, k_B the Boltzmann constant and T the temperature. $\varepsilon_r^{\text{H}_2\text{O}}$ can be derived from Eq. (2) to yield

$$\varepsilon_r^{\text{H}_2\text{O}} = \frac{(C - C_{\text{Poly}})}{C_0}. \quad (4)$$

The particle density Z can also be expressed as the integral of water concentration c in the volume

$$Z(t) = \frac{\int_z \int_y \int_x c(x, y, z, t)\, dx\, dy\, dz \cdot N_A}{V}. \quad (5)$$

For spatially constant concentration ($\nabla c = 0$)

$$Z = \frac{c \cdot V \cdot N_A}{V} = c \cdot N_A \quad . \quad (6)$$

With the help of Eqs. (2), (3) and (6), water concentration can be found as a function of capacitance and temperature:

$$c = \frac{\frac{(C - C_{\text{Poly}})}{C_0} - 1}{\frac{(C - C_{\text{Poly}})}{C_0} + 2} \cdot \frac{3\varepsilon_0}{\alpha + \frac{\mu^2}{k_B T}} \cdot \frac{1}{N_A} \frac{\frac{C - C_{\text{Poly}}}{C_0} - 1}{2 + \frac{C - C_{\text{Poly}}}{C_0}} \cdot \frac{1}{QN_A} \quad . \quad (7)$$

While C is the capacitance actually measured and C_0 is defined as $\varepsilon_0 \frac{A}{d}$, C_{poly} is unknown before calibration. It is estimated by extrapolation of the calibration regression to zero relative humidity. The calibration procedure is described in Sect. 2.4.

2.4 Calibration

Calibration is used to connect the water concentration at the sensor surface c_s to relative humidity in the environment. Diffusion into the polymer will lead to a balance of water concentration c throughout the whole polymer after a finite
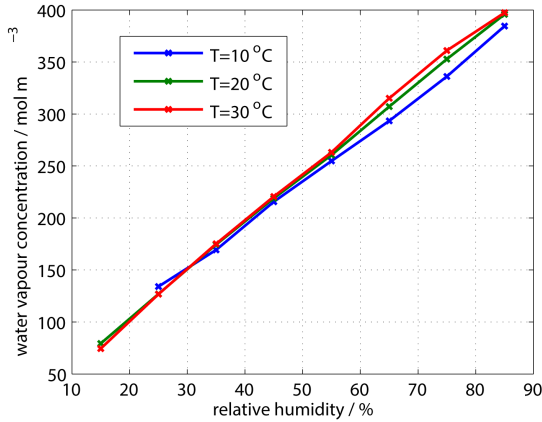
Figure 3. Calibration of a P14 Rapid humidity sensor. Calibration was done at three different temperatures.

time. The dynamics of this process are modelled in Sect. 3. For the calibration, humidity is held at a constant level for at least 30 min to assure equilibrium of the water concentration. It is not necessarily the case that polymer-based capacitive humidity sensors show a linear relationship between measured capacitance and relative humidity (Shibata et al., 1996). Figure 3 shows the result of three calibrations at three different temperatures. On the y axis of the graph, the measured capacitance was directly translated into water vapour concentration, according to Eq. (7). Before doing this, C_{poly} must be set, so that an extrapolation of the curve in Fig. 3 will yield zero water concentration in the polymer at zero ambient relative humidity. A practical way to get a good estimation for C_{poly} is to find the zero-crossing of a regression curve between measured capacitance and relative humidity, which is $(C_{\mathrm{poly}} + C_0)$. Since C_0 is a known sensor property, C_{poly} can be calculated and was found to be approximately 60 pF for the sensor examined here. The temperature in the calibration chamber is kept constant and relative humidity is increased stepwise from 15 to 85 % during the calibration. A dew point mirror in conjunction with a PT100 temperature sensor inside the calibration chamber is used as reference instrument to control relative humidity and temperature. While sensor physics depends on both temperature and water vapour partial pressure, the P14 Rapid follows a linear relationship with relative humidity within the calibrated temperature range. The calibration chamber used was calibrated against a secondary standard with an accuracy of 0.4 % RH. A root mean square error of less than 1 % RH between the calibration curve and the measured values is found for the capacitive humidity sensor calibration in the chamber at 10 °C or more. The facilities that were available to the authors did not allow calibration at lower temperatures.
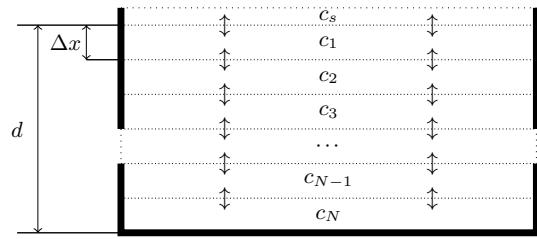
Figure 4. Sketch of the sensor model.

3 Dynamic signal restoration

3.1 Dynamic model

A dynamic model describes the behaviour of a system over time. This behaviour is typically described mathematically by a set of differential equations. In the case of a capacitive humidity sensor, the dynamics are mainly influenced by the diffusion of water vapour from the sensor surface into the polymer. While the water concentration c in the polymer was constant in space in the stationary model described in Sect. 2.3, the following section will describe how the concentration changes in time and space. The diffusion flux $\mathbf{J}$ is described by Fick's law as shown in Eq. (8). It is assumed that a model with a spatially constant diffusion coefficient D describes the behaviour of the sensor well enough. Figure 4 shows a sketch of the model of finite volumes in the sensor polymer.

$$\mathbf{J} = -D \cdot \nabla c \tag{8}$$

Combined with the continuity equation of mass conservation (Eq. 9), Fick's second law can be derived (Eq. 10).

$$\frac{\partial c}{\partial t} = -\nabla \cdot \mathbf{J} \tag{9}$$

$$= D \, \nabla^2 c \tag{10}$$

Since these equations yield a differential equation of second order, a simplification is needed to find a manageable solution. A common solution to these kinds of problems is a numerical approach, such as the finite-volume method (LeVeque, 2002). According to this method, the mass conservation Eq. (9) is integrated over a finite-volume element V_n.

$$\iiint_{V_n} \frac{\partial c}{\partial t} \, \mathrm{d}V = - \iiint_{V_n} (\nabla \cdot \mathbf{J}) \, \mathrm{d}V \tag{11}$$

The divergence theorem (or the combination of the continuity equation with the Gauss theorem) allows one to write the right-hand side of the equation as a surface integral. The left-hand side can be solved to obtain the product of spatially averaged concentration change in a volume element and its volume.

$$\frac{\partial \overline{c_n}}{\partial t} V_n = - \oiint_s \mathbf{J} \, \mathrm{d}S \tag{12}$$

In the following, concentrations with an index always represent spatial averages over a finite volume, and the overbar notation to indicate the averaging, as in $\overline{c_n}$, will be omitted. Concentration gradients in horizontal directions are considered to be 0, as the sensor is small enough that a constant humidity above the whole sensor surface can be assumed. Therefore, there will be no horizontal fluxes of water and the volume elements V_n can be simplified to layers as shown in Fig. 4. The surface integral can be simplified to the sum of diffusion from the layer above $(n-1)$ and the layer below $(n+1)$ for each layer n in the polymer and therefore yields

$$\frac{\partial c_n}{\partial t} = \frac{-D \cdot \frac{c_n - c_{n-1}}{\Delta x} \cdot A_{n,n-1}}{V_n} + \frac{-D \cdot \frac{c_n - c_{n+1}}{\Delta x} \cdot A_{n,n+1}}{V_n}, \quad (13)$$

where $A_{n,n-1}$ and $A_{n,n+1}$ are the top and bottom surface area of the polymer layers respectively and Δx is the layer thickness. A matrix representation of the simplified diffusion model with $\mathbf{Y} = \frac{D \cdot A}{\Delta x \cdot V_n}$ is given in Eq. (14).

$$
\begin{pmatrix} \frac{\partial c_1}{\partial t} \\ \frac{\partial c_2}{\partial t} \\ \frac{\partial c_3}{\partial t} \\ \frac{\partial c_4}{\partial t} \\ \vdots \\ \vdots \\ \frac{\partial c_{N-1}}{\partial t} \\ \frac{\partial c_N}{\partial t} \end{pmatrix}
=
\begin{pmatrix}
-2Y & Y & 0 & 0 & 0 & 0 & \cdots & 0 \\
Y & -2Y & Y & 0 & 0 & 0 & \cdots & 0 \\
0 & Y & -2Y & Y & 0 & 0 & \cdots & 0 \\
0 & 0 & Y & -2Y & Y & 0 & \cdots & 0 \\
\vdots & & & & \ddots & & & \vdots \\
\vdots & & & & & \ddots & & \vdots \\
0 & 0 & 0 & 0 & \cdots & Y & -2Y & -Y \\
0 & 0 & 0 & 0 & \cdots & 0 & Y & -Y
\end{pmatrix}
$$
$$
\cdot
\begin{pmatrix} c_1 \\ c_2 \\ c_3 \\ c_4 \\ \vdots \\ \vdots \\ c_{N-1} \\ c_N \end{pmatrix}
+
\begin{pmatrix} Y \\ 0 \\ 0 \\ 0 \\ \vdots \\ \vdots \\ 0 \\ 0 \end{pmatrix}
\cdot c_s
$$
$$
c_m = (1\ 1\ 1\ \cdots\ 1)
\begin{pmatrix} \frac{c_1}{N} \\ \frac{c_2}{N} \\ \frac{c_3}{N} \\ \frac{c_4}{N} \\ \vdots \\ \frac{c_N}{N} \end{pmatrix}
\quad (14)
$$

Boundary conditions exist for the layer at the surface of the sensor and the bottommost layer. At the surface layer the concentration that is adsorbed from ambient water vapour diffuses into the layer. At the bottom, no diffusion is possible from below.

Equation (14), translated to vector notation, conforms with the standard layout of a single-input–single-output (SISO) state–space model as used in control theory (Lutz and Wendt, 2007):

$$\frac{\partial}{\partial t} c = \mathbf{Y}c + (Y\ 0\ 0\ \cdots\ 0)^T c_s$$

$$c_m = \left(\frac{1}{N}\ \frac{1}{N}\ \frac{1}{N}\ \cdots\ \frac{1}{N} \right) c. \quad (15)$$
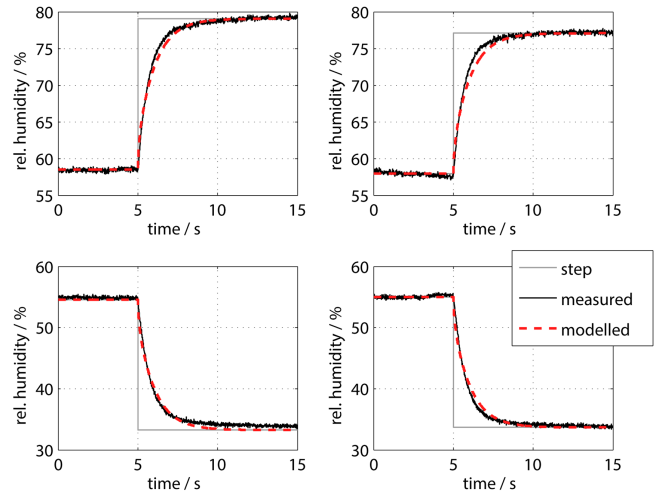
Figure 5. Result of a step response experiment with rising-edge (upper figures) and falling-edge (lower figures) humidity in comparison to model results. The model was run with 40 layers and a diffusion coefficient $D = 0.38\,\mu\text{m}^2\,\text{s}^{-1}$ in all cases.

The vector c of water concentrations in each layer of the model is the state vector. The diffusion matrix $\mathbf{Y}$ is the system (or state) matrix, which describes how the current concentrations c in each layer affect the change in concentrations $\frac{\partial}{\partial t} c$. The input (or control) vector $(Y\ 0\ 0\ \cdots\ 0)^T$ determines how the system input affects the states c. It is modelled to describe the diffusion of water vapour into the topmost layer of the sensor. The single-input variable of the whole system is the surface concentration c_s and the single output variable is the averaged water concentration in the polymer c_m that is presented as a function of the measured capacitance in Eq.(7). The so-called output vector $\left(\frac{1}{N}\ \frac{1}{N}\ \frac{1}{N}\ \cdots\ \frac{1}{N} \right)$ maps the states c to the output variable c_m, which, in the case of the sensor model, is a simple averaging of the concentrations in all layers.

3.1.1 Model validation

To show that this model does agree with reality, step response experiments with rising and falling edge steps of humidity were performed. The results in Fig. 5 show that the model agrees well with reality if the correct diffusion coefficient is applied. Of course, it has to be noted that the diffusion coefficient, since it is the one unknown parameter in the model, also serves as a correction factor for other model inaccuracies and therefore is most likely not the true physical diffusion coefficient. Remaining deviations between model and measurement can also result from a nonperfect step input. For the experiment, a humidity sensor was placed in a very small chamber ($< 2\,\text{cm}^3$) at ambient humidity. At time 0 the constant airflow into the chamber is switched to an airflow of well-defined humidity from the dew point generator, which is also used for calibration. It is assumed that the humidity around
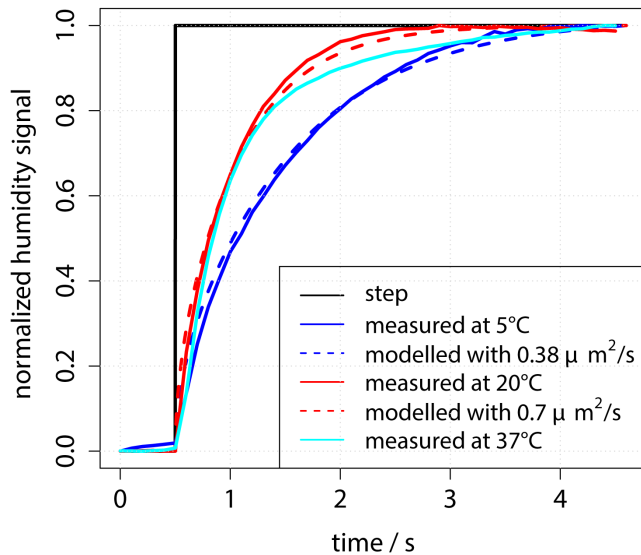
Figure 6. Step responses of the same sensor at different temperatures. The y axis is normalized to 0 for humidity before the step and 1 for humidity after the step. This is legitimate since the dynamics does not depend on the step amplitude.

the sensor changes completely in less than 100 ms, based on the outlet flow of the generator and the size of the chamber. Comparing the rising and falling edge steps, it becomes evident that no difference in time response can be observed for both cases, and the model works with the same diffusion coefficient without hysteresis. This implies that diffusion is the dominant factor in comparison to adsorption and desorption regarding the dynamics of the sensor, and the model is suitable for describing the dynamic behaviour of the sensor.

To investigate the sensitivity of the diffusion coefficient to ambient temperature, tests were done at three different temperatures (5, 20 and 37 °C). The result in Fig. 6 shows that the diffusion coefficient at 5 °C is lower compared to the other two temperatures, which agree quite well. This means that it is not possible to apply a universal diffusion coefficient for one sensor, but the diffusion coefficient needs to be adapted to the given ambient temperature, especially in low-temperature environments. However, small deviations as they appear in the ABL will not be critical for the model.

3.2 Inverse model for signal restoration

Having found a model that reasonably describes the dynamic behaviour of the sensor, it is now possible to use this model to restore the original signal of relative humidity in the atmosphere from measured data. For this purpose it is necessary to invert the model, which is equivalent to solving the system equations for the surface water vapour concentration c_s.

Since the state–space model cannot easily be inverted, the first step is to transform Eq. (15) to a transfer function in the Laplace domain. This can be done as presented in Eq. (16)

according to Lutz and Wendt (2007).

$$c_m(s) = \left(\frac{1}{N} \ \frac{1}{N} \ \cdots \ \frac{1}{N} \right) (s\mathbf{E} - \mathbf{Y})^{-1} (Y \ 0 \cdots 0)^T \cdot c_s(s)$$
$$= G(s) \cdot c_s(s) \tag{16}$$

$\mathbf{E}$ is a unity matrix of the same dimensions as the system matrix $\mathbf{Y}$. The variable s is a result of the Laplace transformation. $G(s)$ is the transfer function in the Laplace domain. A transfer function of a linear dynamic system can be expressed as a fraction with a numerator and a denominator polynomial of the parameter s in the Laplace domain (Astrom and Murray, 2009, chapter 8). This fraction can simply be inverted to solve Eq. (16) for the original signal:

$$c_s(s) = G(s)^{-1} \cdot c_m(s). \tag{17}$$

A drawback of this method is that it only works well if the measured signal and the applied model fit well. Noise that is not modelled will be amplified more with increasing polynomial order in the transfer function. On the other hand, the model will be more accurate with a higher number of modelled layers in the polymer, which leads to a high polynomial order in the transfer function. A way of dealing with this problem is oversampling and careful filtering of the measured signal in order to achieve a good signal-to-noise ratio.

Figure 7 shows a signal flow block diagram (see, e.g., Astrom and Murray, 2009, pp. 55–59) of the signal restoration. It includes input and output filters that were applied to achieve a restored signal that is not disturbed by amplified noise of the inverse modelling. For the input, a sharp low-pass filter of 20th order at a cutoff frequency of 10 Hz is chosen to eliminate the white noise of the capacitance measurement, which dominates above this frequency. In the output filter, a first-order low pass is good enough to filter out the remaining noise after the signal restoration. The block diagram was generated with Matlab Simulink®, which was also used in a first approach to carry out the convolution of the measured signal with the transfer function.

4 Results

4.1 Vertical profiles

For vertical profiles, slow dynamics of sensors lead to blurred measurements with either overestimated or underestimated water vapour concentration at each altitude, depending on the lapse rate. The effect shows clearly whether RPA flights are used with consecutive ascents and descents. The sensor dynamics result in a hysteresis between ascent and descent measurement of relative humidity. In the past it was common practice to take the average of ascent and descent flights, which gives a good approximation for the true value, or to apply some time delay correction of first order as described in Jonassen (2008) for RPA and in Leiterer et al. (2005) and Miloshevich et al. (2004) for radiosondes.
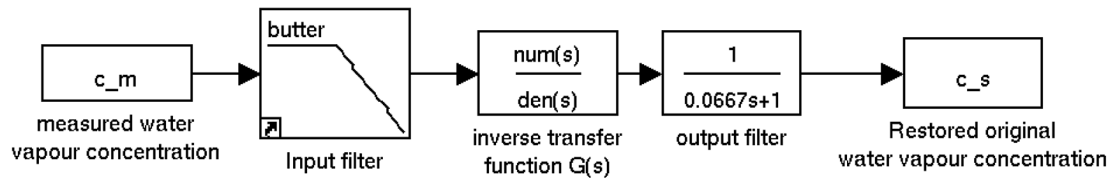
Figure 7. Block diagram of signal restoration. The input signal of the humidity sensor is filtered with a Butterworth filter of order 20 at a cutoff frequency of 10 Hz. After the inverse transformation, the signal is filtered again with a simple first-order delay low pass with cutoff frequency at 15 Hz.
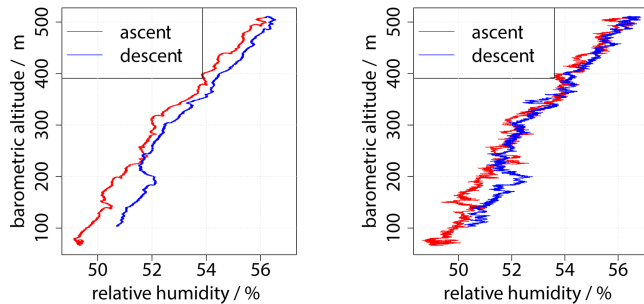
Figure 8. Vertical profile of relative humidity before and after correction.

Figure 9. Power spectrum of relative humidity before and after correction. The number of layers in the sensor model is set to $N = 40$. From the vertical profile, the diffusion constant was found to be $D = 0.1\,\mu m^2\,s^{-1}$. The spectrum is averaged over five flight legs.

In Fig. 8, a vertical profile is shown with raw measurements and with a restored signal for relative humidity, applying the method described in Sect. 3. It clearly shows how an offset present between ascent and descent of the flight is eliminated in almost every detail, except for a few altitudes, where obviously local events of water vapour disturb the continuity of the profile, as can be seen between 150 and 200 m or at 350 m barometric altitude. The parameter that is critical to tune in the sensor model is the diffusion coefficient as described above. Within the minute or two that are needed for an ascent and a descent of a vertical profile with the RPA, in a nonconvective boundary layer, the mean relative humidity will not shift into one direction or the other, so that the parameter can be tuned to show a minimum offset between ascent and descent. Once the diffusion coefficient is found from a vertical profile, it is possible to use this parameter for the signal restoration of the complete flight with a duration of 30–60 min. It is, however, recommended to redo the vertical profile diffusion coefficient estimation for each flight since contamination and small damage invisible to the human eye were found to significantly change the sensor dynamics. Different sensors of the same batch can even show slightly different characteristics. Of course, this way of determining the diffusion coefficient only works if gradients of water vapour concentration do exist at least in parts of the vertical profile.

4.2 Spectral response

A MASC RPA at the University of Tübingen is equipped with fast sensors for temperature and wind measurement in order to measure turbulence. The goal of this study is to make turbulence studies for water vapour possible with capacitive humidity sensors. To quantify the improvements that were achieved in working towards this goal, it is useful to investigate the spectral response of the sensor before and after the signal restoration. Figure 9 shows the power spectral density of the relative-humidity signal over the frequency for both cases. The original signal is strongly effected by the slow sensor dynamics for frequencies above 0.05 Hz (red curve). At about 3 Hz the signal vanishes in noise entirely (spectral power is almost constant for higher frequencies). The restored signal almost perfectly follows the expected $-5/3$ slope for locally isotropic turbulence in the inertial subrange according to Kolmogorov (1941), until about 3 Hz (blue curve). For higher frequencies, noise is dominant and thus is the limiting factor of the signal restoration.

Another method to show the distribution of turbulent energy on different scales is the structure function according to Kolmogorov (1941). Deviations of the measured values from the theoretical slope for locally isotropic turbulence in the inertial subrange, which in the case of the double-logarithmically plotted structure function is 2/3, are a strong
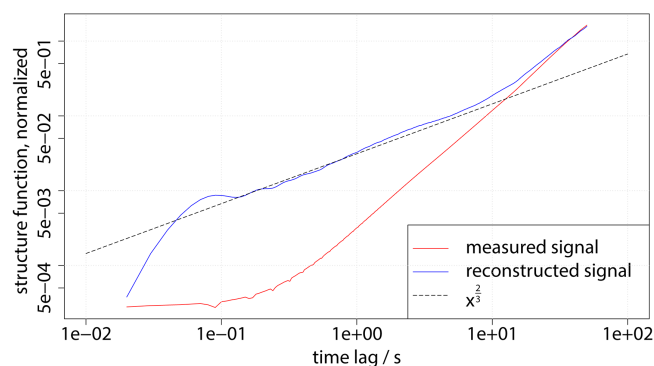
Figure 10. Structure function before and after correction. The number of layers in the sensor model is set to $N = 40$. The diffusion constant was found to be $D = 0.1\,\mu\mathrm{m}^2\,\mathrm{s}^{-1}$ from the vertical profile. The structure function is normalized by $2\sigma^2$ and averaged over five flight legs.

indication of sensor dynamics or other errors in the measurement; this is the case even more clearly than for the power spectral densities. Figure 10 shows how close the structure function of the restored signal is to the theory until a time lag of about 0.3 s (corresponding to 3 Hz), especially compared to the original signal.

5 Conclusions

This report addressed the problem of water vapour measurement for turbulence analysis with small RPA. It was established that capacitive humidity sensors are currently the only feasible solution for these measurements onboard an RPA of 5 kg, as operated in Tübingen, or smaller. A method is introduced to enhance the quality of such measurements with the help of control theory methods in post-processing. The dynamic diffusion model derived in Sect. 3 is therefore inverted to find the water concentration on the sensor surface from measured average water concentration in the polymer. Since the measurement variable of the sensor is, in the first place, the capacitance, the physics of how to translate the measured capacitance into water concentration was introduced in Sect. 2.3. A calibration approach was used to connect sensor surface water concentration to ambient relative humidity (Sect. 2.4). To summarize, the model can be applied in five steps:

1. calculation of average water concentration in the polymer c_m for a time series of capacitance of the sensor according to Sect. 2.3;

2. setup of the state–space model according to Sect. 3.1;

3. conversion of the state–space model into a transfer function according to Sect. 3.2, Eq. (16);

4. deconvolution of the measured average water concentration signal c_m in the polymer with the transfer function in order to find the water concentration at the surface of the polymer c_s (Eq. 17);

5. recovery of the relative humidity from the surface water concentration c_s through the calibration described in Sect. 2.4.

It is shown in Sect. 4 how vertical profiles can be corrected using the presented method. We propose using a minimization of error between ascent and descent of a vertical profile flight with an RPA to find the correct diffusion coefficient for the given temperature and sensor. This is necessary, since the exact relation between diffusion coefficient and temperature could not be determined in a laboratory experiment and information about the polymer type is not available. The benefit of determining the diffusion coefficient empirically for each measurement flight is that this parameter is the only unknown in the dynamic model and therefore can also be used to correct for other inaccuracies in the model. A spectral analysis of flight legs in the atmospheric boundary layer with a diffusion coefficient determined from a vertical profile during the same flight showed promising results for turbulence analysis. It can be stated that the enhancement of the sensor makes it possible to resolve turbulent fluctuations up to 3 Hz, which corresponds to a 10 m eddy size at $25\,\mathrm{m\,s}^{-1}$ airspeed. Compared to temperature and wind measurement on a MASC RPA (up to 20 Hz), this is still fairly low and will need to be improved in future work. The main constraints for the given setup are the signal-to-noise ratio and the sensitivity of the capacitance measurement. Improvements of the measurement circuit with several parallel sensors can possibly solve this problem. Measurements of turbulent fluctuations up to 10 Hz seem possible. The systematic approach of the signal restoration is open to further extensions of the sensor model, e.g. physical descriptions of water adsorption on the sensor surface or temperature dependence of diffusion into the polymer. These extensions can lead to significantly higher complexity, which cannot be described by a linear time-invariant system any more. For measurements in the summer convective boundary layer in central Europe, the described simplifications are appropriate and provide promising results. To apply the method in very cold temperatures or in radiosonde applications, where strong temperature differences are experienced in a single ascent, further studies that are beyond of the scope of this paper are required.

Edited by: M. Hamilton

References

Astrom, K. and Murray, R.: Feedback Systems: An Introduction for Scientists and Engineers, Princeton University Press, 2009.

Bange, J. and Roth, R.: Helicopter-Borne Flux Measurements in the Nocturnal Boundary Layer Over Land – a Case Study, Bound.-Lay. Meteorol., 92, 295–325, 1999.

Bange, J., Beyrich, F., and Engelbart, D. A. M.: Airborne Measurements of Turbulent Fluxes during LITFASS-98: A Case Study about Method and Significance, Theor. Appl. Climatol., 73, 35–51, 2002.

Bange, J., Esposito, M., and Lenschow, D. H.: Airborne Measurements for Environmental Research – Methods and Instruments, chap. 2: Measurement of Aircraft State, Thermodynamic and Dynamic Variables, 641 pp., Wiley, 2013.

Buck, A. L.: The Variable-Path Lyman-Alpha Hygrometer and Its Operating Characteristics, Bull. Am. Meteorol. Soc., 57, 1113–1118, 1976.

Campbell, G., Tanner, B., and Gauthier, R.: Krypton hygrometer, available at: http://www.google.com/patents/US4526034 (last access: 17 September 2014), uS Patent 4,526,034, 1985.

Chao, H., Baumann, M., Jensen, A., Chen, Y., Cao, Y., Ren, W., and McKee, M.: Band-reconfigurable multi-UAV-based cooperative remote sensing for real-time water management and distributed irrigation control, IFAC World Congress, Seoul, Korea, 2008.

Corsmeier, U., Hankers, R., and Wieser, A.: Airborne Turbulence Measurements in the Lower Troposphere Onboard the Research Aircraft Dornier 128-6, D-IBUF, Meteorol. Z., 4, 315–329, 2001.

Debye, P.: Polare Molekeln, S. Hirzel, Leipzig, 200 pp., 1929.

Eckles, R.: Gas analyzer, available at: http://www.google.com/patents/US6317212 (last access: 17 September 2014), uS Patent 6,317,212, 2001.

Garratt, J.: The Atmospheric Boundary Layer, University Press, Cambridge, 1992.

IST AG: P14 – Rapid Capacitive Humidity Sensor, datasheet V4.3-11/2009, 2009.

Jensen, A. and Chen, Y.: Tracking tagged fish with swarming unmanned aerial vehicles using fractional order potential fields and Kalman filtering, in: 2013 International Conference on Unmanned Aircraft Systems (ICUAS), 1144–1149, IEEE, 2013.

Jonassen, M. O.: The Small Unmanned Meteorological Observer (SUMO), Master's thesis, University of Bergen – Geophysical Institute, 2008.

Kolmogorov, A.: The Local Structure of Turbulence in Incompressible Viscous Fluid for Very Large Reynolds Numbers, Dokl. Akad. Nauk SSSR, 30, 299–303, reprint: Proc. R. Soc. Lond. A, 1991, 434, 9–13, 1941.

Kuisma, H., Lehto, A., and Jalava, J.: Capacitive humidity sensor and method for the manufacture of same, available at: http://www.google.com/patents/US4500940 (last access: 17 September 2014), uS Patent 4,500,940, 1985.

Leiterer, U., Dier, H., Nagel, D., Naebert, T., Althausen, D., Franke, K., Kats, A., and Wagner, F.: Correction Method for RS80-A Hu-

micap Humidity Profiles and Their Validation by Lidar Backscattering Profiles in Tropical Cirrus Clouds, J. Atmos. Oceanic Technol., 22, 18–29, 2005.

LeVeque, R. J.: Finite Volume Methods for Hyperbolic Problems, Cambridge University Press, doi:10.1017/CBO9780511791253, 2002.

Lutz, H. and Wendt, W.: Taschenbuch der Regelungstechnik: mit MATLAB und Simulink, Harri Deutsch, Frankfurt am Main, Germany, 2007.

Maronga, B.: Monin-Obukhov similarity functions for the structure parameters of temperature and humidity in the unstable surface layer: results from high-resolution large-eddy simulations, J. Atmos. Sci., 71, 716–733, doi:10.1175/JAS-D-13-0135.1, 2013.

Martin, S. and Bange, J.: The Influence of Aircraft Speed Variations on Sensible Heat Flux Measurements by Different Airborne Systems, Bound.-Lay. Meteorol., 150, 153–166, doi:10.1007/s10546-013-9853-7, 2013.

Martin, S., Bange, J., and Beyrich, F.: Meteorological profiling of the lower troposphere using the research UAV "M2AV Carolo", Atmos. Meas. Tech., 4, 705–716, doi:10.5194/amt-4-705-2011, 2011.

Martin, S., Beyrich, F., and Bange, J.: Observing Entrainment Processes Using a Small Unmanned Aerial Vehicle: A Feasibility Study, Bound.-Lay. Meteorol., 150, 449–467, doi:10.1007/s10546-013-9880-4, 2013.

May, R. D.: Open-path, near-infrared tunable diode laser spectrometer for atmospheric measurements of H_2O, J. Geophys. Res.-Atmos., 103, 19161–19172, doi:10.1029/98JD01678, 1998.

Miloshevich, L. M., Paukkunen, A., Vömel, H., and Oltmans, S. J.: Development and Validation of a Time-Lag Correction for Vaisala Radiosonde Humidity Measurements, J. Atmos. Oceanic Technol., 21, 1305–1327, doi:10.1175/jtech1770.1, 2004.

Neininger, B., Fuchs, W., Baeumle, M., Volz-Thomas, A., Prévôt, A. S. H., and Dommen, J.: A Small Aircraft for More Than Just Ozone: MetAir's 'Dimona' After Ten Years of Evolving Development, in: 11th Symp. on Meteorological Observations and Instrumentation, Albuquerque, NM, Amer. Meteor. Soc., 123–128, 2001.

Paige, M. E.: Compact and Low-Power Diode Laser Hygrometer for Weather Balloons, J. Atmos. Oceanic Technol., 22, 1219–1224, doi:10.1175/jtech1770.1, 2005.

Rediniotis, O. and Pathak, M.: Simple Technique for Frequency-Response Enhancement of Miniature Pressure Probes, AIAA Journal, 37, 897–899, 1999.

Reuder, J., Brisset, P., Jonassen, M., Müller, M., and Mayer, S.: The Small Unmanned Meteorological Observer SUMO: A new tool for atmospheric boundary layer research, Meteorol. Z., 18, 141–147, 2009.

Sen, A. and Darabi, J.: Modeling and Optimization of a Microscale Capacitive Humidity Sensor for HVAC Applications, Sensors Journal, IEEE, 8, 333–340, 2008.

Shibata, H., Ito, M., Asakursa, M., and Watanabe, K.: A digital hygrometer using a polyimide film relative humidity sensor, IEEE Trans. Instr. Measure., 45, 564–569, 1996.

Spieß, T., Bange, J., Buschmann, M., and Vörsmann, P.: First Application of the Meteorological Mini-UAV "M2AV", Meteorol. Z. N. F., 16, 159–169, 2007.

Stull, R.: An Introduction to Boundary Layer Meteorology, Kluwer Acad., Dordrecht, 1988.

Tagawa, M., Kato, K., and Ohta, Y.: Response compensation of fine-wire temperature sensors, Rev. Sci. Instrum., 76, 094904, 4 pp., 2005.

Tetelin, A. and Pellet, C.: Modeling and optimization of a fast response capacitive humidity sensor, Sensors Journal, IEEE, 6, 714–720, 2006.

Thomas, R. M., Lehmann, K., Nguyen, H., Jackson, D. L., Wolfe, D., and Ramanathan, V.: Measurement of turbulent water vapor fluxes using a lightweight unmanned aerial vehicle system, Atmos. Meas. Tech., 5, 243–257, doi:10.5194/amt-5-243-2012, 2012.

van den Kroonenberg, A., Martin, S., Beyrich, F., and Bange, J.: Spatially-averaged temperature structure parameter over a heterogeneous surface measured by an unmanned aerial vehicle, Bound.-Lay. Meteorol., 142, 55–77, 2011.

van den Kroonenberg, A. C., Martin, T., Buschmann, M., Bange, J., and Vörsmann, P.: Measuring the Wind Vector Using the Autonomous Mini Aerial Vehicle M^{2}AV, J. Atmos. Oceanic Technol., 25, 1969–1982, 2008.

Wildmann, N., Mauz, M., and Bange, J.: Two fast temperature sensors for probing of the atmospheric boundary layer using small remotely piloted aircraft (RPA), Atmos. Meas. Tech., 6, 2101–2113, doi:10.5194/amt-6-2101-2013, 2013.

Wildmann, N., Ravi, S., and Bange, J.: Towards higher accuracy and better frequency response with standard multi-hole probes in turbulence measurement with remotely piloted aircraft (RPA), Atmos. Meas. Tech., 7, 1027–1041, doi:10.5194/amt-7-1027-2014, 2014.

Wyngaard, J. C. and Clifford, S. F.: Estimating Momentum, Heat, and Moisture Fluxes from Structure Parameters, J. Atmos. Sci., 35, 1204–1211, 1978.

Zondlo, M. A., Paige, M. E., Massick, S. M., and Silver, J. A.: Vertical cavity laser hygrometer for the National Science Foundation Gulfstream-V aircraft, J. Geophys. Res., 115, D20309, doi:10.1029/2010JD014445, 2010.